Published February 24, 2014

Fission of SNX-BAR–coated endosomal retrograde transport carriers is promoted by the dynamin-related protein Vps1

Richard J. Chi,[1] Jingxuan Liu,[1] Matthew West,[2] Jing Wang,[1] Greg Odorizzi,[2] and Christopher G. Burd[1]

[1]Department of Cell Biology, Yale School of Medicine, New Haven, CT 06520
[2]Department of Molecular, Cellular, and Developmental Biology, University of Colorado, Boulder, Boulder, CO 80309

Retromer is an endosomal sorting device that orchestrates capture and packaging of cargo into transport carriers coated with sorting nexin BAR domain proteins (SNX-BARs). We report that fission of retromer SNX-BAR–coated tubules from yeast endosomes is promoted by Vps1, a dynamin-related protein that localizes to endosomes decorated by retromer SNX-BARs and Mvp1, a SNX-BAR that is homologous to human SNX8. Mvp1 exhibits potent membrane remodeling activity in vitro, and it promotes association of Vps1 with the endosome in vivo. Retrograde transport carriers bud from the endosome coated by retromer and Mvp1, and cargo export is deficient in *mvp1*- and *vps1*-null cells, but with distinct endpoints; cargo export is delayed in *mvp1*-null cells, but cargo export completely fails in *vps1*-null cells. The results indicate that Mvp1 promotes Vps1-mediated fission of retromer- and Mvp1-coated tubules that bud from the endosome, revealing a functional link between the endosomal sorting and fission machineries to produce retrograde transport carriers.

Introduction

The endosomal system is composed of an interconnected network of related organelles that function primarily in the dissociation and sorting of proteins and ligands. Cargo proteins in the early/sorting endosome are either retained during endosome maturation and delivered to the lysosome, or exported from the endosome and delivered to other organelles for reuse. As sorting underlies the physiological functions of the endosomal system, the elucidation of transport carrier biogenesis mechanisms is key for a fundamental understanding of the endosomal system and also the etiology of diseases that arise from loss or misregulation of endosome function.

The topological features of endosome membranes are intimately linked to cargo-sorting reactions. As endosomes mature, they accrue intraluminal vesicles (ILVs) and a network of tubules are drawn from the vacuolar domain (Roth and Porter, 1964; Geuze et al., 1983; Hopkins, 1983) that has been referred to as the "compartment of uncoupling of receptor and ligand" (Geuze et al., 1983) or, more recently, the "tubular endosomal network" (TEN; Bonifacino and Rojas, 2006). Whereas integral membrane proteins that are retained within the endosome are packaged into ILVs, recycling and retrograde cargo is packaged into the TEN or vesicles that bud into the cytoplasm and undergo fission. Sorting of recycling/retrograde cargo is mediated by soluble proteins that are recruited to the endosome membrane where they recognize sorting signals in the cargo, but the mechanisms of transport carrier formation and fission are poorly understood. One class of endosomal coat proteins proposed to mediate packaging of endosomal cargo are sorting nexin (SNX) proteins containing a Bin-Amphiphysin-Rvs (BAR) domain (Teasdale and Collins, 2012) that displays a curved membrane binding surface and can oligomerize. In addition, SNX-BAR proteins possess a PHOX homology (PX) domain that recognizes phosphatidylinositol 3-phosphate, a lipid that is enriched on endosome membranes, and through the combined membrane-binding activities of SNX-BAR protein domains many can recognize PtdIns3*P*-containing high positive curvature membranes, such as those comprising the tubular endosomal network. Recent work cataloged oligomeric interactions of 12

Correspondence to Christopher G. Burd: christopher.burd@yale.edu

J. Liu's present address is Department of Medical Oncology, Dana Farber Cancer Institute, Boston, MA 02115.

Abbreviations used in this paper: BAR, Bin-Amphiphysin-Rvs161; CPY, carboxypeptidase Y; ILV, intraluminal vesicle; MVB, multivesicular body; PX, Phox homology; SNX, sorting nexin; TEN, tubular endosomal network.

© 2014 Chi et al. This article is distributed under the terms of an Attribution–Noncommercial–Share Alike–No Mirror Sites license for the first six months after the publication date (see http://www.rupress.org/terms). After six months it is available under a Creative Commons License (Attribution–Noncommercial–Share Alike 3.0 Unported license, as described at http://creativecommons.org/licenses/by-nc-sa/3.0/).

Supplemental Material can be found at:
http://jcb.rupress.org/content/suppl/2014/03/03/jcb.201309084.DC2.html
http://jcb.rupress.org/content/suppl/2014/02/21/jcb.201309084.DC1.html

The Rockefeller University Press $30.00
J. Cell Biol. Vol. 204 No. 5 793–806
www.jcb.org/cgi/doi/10.1083/jcb.201309084

THE JOURNAL OF CELL BIOLOGY

Downloaded from jcb.rupress.org on June 24, 2015

Published February 24, 2014

human SNX-BARs and found that a subset of them can drive the formation of tubules in vitro via homo-oligomerization, suggesting that each type of higher order SNX-BAR oligomer could function on a distinct, cargo-specific export pathway (van Weering et al., 2012a). In support of this, in cultured metazoan cells expressing fluorescently tagged SNX1 and SNX4, tubules emanating from a vacuolar endosome are observed to be decorated with one or the other, but not both (Traer et al., 2007). However, it is not yet resolved if this is a general feature of all SNX-BAR proteins.

Retromer was discovered in studies using budding yeast (*Saccharomyces cerevisiae*) and was originally defined as a pentameric complex containing the Vps26–Vps29–Vps35 trimer and a heterodimer of the Vps5 and Vps17 SNX-BAR proteins (Seaman et al., 1997, 1998). There are at least six yeast SNX-BAR proteins encoded by the yeast genome, but Vps5 and Vps17 are the only ones that co-purify with retromer, and in human cells there are four retromer-associated SNX-BAR proteins (SNX1, SNX2, SNX5, and SNX6), but the human SNX-BARs do not associate with the retromer trimer as robustly as the yeast retromer SNX-BARs do, so it has been challenging to strictly define the SNX-BAR components of retromer pathways in human cells. A yeast SNX-BAR called Mvp1 has also been described that is the putative orthologue of the human SNX8 protein (Ekena and Stevens, 1995). Cells deleted of the *MVP1* gene exhibit protein-sorting deficiencies that are nearly as severe as those observed in retromer-null mutants (Ekena and Stevens, 1995; Bonangelino et al., 2002), raising the possibility that Mvp1/Snx8 is a key component of the retromer pathway. Insight into the function of Mvp1 is further provided by the finding that increased gene dosage of *MVP1* (multi-copy suppressor of *vps1*^{d}) partially ameliorates the protein-sorting defects caused by expression of a dominant-negative *vps1* allele (Ekena and Stevens, 1995). *VPS1* encodes a dynamin family GTPase implicated in fission of transport vesicles at the Golgi, endosome, and plasma membrane. In this study we report that Mvp1 is required for efficient cargo export from the endosome by retromer, and that Vps1 is required for fission of cargo-containing, SNX-BAR–coated tubules from the endosome.

Results

Mvp1 is broadly localized within the endosomal system

Mvp1 was originally proposed to function in the Golgi apparatus (Ekena and Stevens, 1995), but the putative human orthologue of Mvp1, called SNX8, localizes to endosomes in human cells (Dyve et al., 2009; van Weering et al., 2012b), prompting us to reevaluate Mvp1 localization. Mvp1-GFP decorates 3–10 puncta per cell, often near the vacuole, as well as the cytosol (Fig. S1 A). Localization to these puncta is disrupted by loss of the sole PI3K (*vps34*Δ) and by a mutation, R172A, in the PtdIns3*P* binding pocket of its PX domain, suggesting that Mvp1 localizes to PtdIns3*P*. We further characterized these organelles by comparing Mvp1 localization to three other sorting nexins: Snx4-GFP, generally considered to function on early endosomes and the preautophagosome structure (Hettema et al., 2003), Vps17-mCherry, a retromer SNX-BAR generally considered to decorate prevacuolar endosomes, and Snx3-GFP, a PX-only sorting nexin that functions with retromer (Fig. S1 B). All tagged proteins were expressed from their native loci and colocalization was assessed using Pearson's correlation coefficients (R; Fig. S1 B). Although there are positive correlations with all endosome markers tested, the highest correlation ($R_{ave} = 0.40$) is observed with the retromer SNX-BAR, Vps17, indicating that Mvp1 localizes throughout the endosomal system, but is enriched on retromer-decorated endosomes. The human orthologue of Mvp1, SNX8, also localizes to retromer-decorated endosomes (Dyve et al., 2009; van Weering et al., 2012b).

Failure of retromer-mediated cargo export in *mvp1*Δ cells

The vacuolar protein sorting receptor, Vps10, traffics newly synthesized vacuolar carboxypeptidase Y (CPY) from the TGN to the endosome, and is then retrieved to the TGN via the retromer pathway (Seaman et al., 1997). In retromer mutants, Vps10 fails to be retrieved and, as a consequence, ∼80% of newly synthesized CPY is secreted from the cell (Seaman et al., 1997; Bonangelino et al., 2002). Null *mvp1*Δ cells secrete 65% of newly synthesized CPY (Ekena and Stevens, 1995; Bonangelino et al., 2002); however, the basis of this sorting defect is unknown. To directly test for a role for Mvp1 in endosome-to-TGN retrieval of Vps10, we examined Vps10-GFP in wild-type and *mvp1*Δ cells (Fig. 1 A). In wild-type cells Vps10-GFP localizes to 10–20 puncta representing Golgi and endosome compartments, identified by colocalization with Sec7 (as a tomato dimer fusion, "tom"), a marker of the TGN, or the Vps17 retromer SNX-BAR (i.e., Vps17-tom). In *mvp1*Δ cells Vps10-GFP localizes to fewer punctate organelles (Fig. 1 A) and more of it appears to colocalize with Vps17-tom than in wild-type cells (Fig. 1 A), leading us to speculate that Vps10 accumulates in retromer-decorated endosomes in *mvp1*Δ cells. To rigorously test this, we quantified the absolute amounts of Vps10-GFP in the Golgi and the endosome. Because standard fluorescence intensity correlation analyses (e.g., Pearson's, Mander's) do not provide an absolute measure of Vps10-GFP distribution, we devised a method de novo to determine the amounts of Vps10-GFP that localize to late Golgi compartments decorated by Sec7 and to endosomes decorated by the Vps17 retromer SNX-BAR. The results (Fig. 1 B) show that in wild-type cells, 58% of Vps10-GFP molecules localize to the Golgi (i.e., are contained within the Sec7-tom mask), and 23% localize to retromer-decorated endosomes (i.e., are contained within the Vps17-tom mask). In striking contrast to this distribution, in *mvp1*Δ cells 36% of Vps10-GFP localizes to the Golgi, and there is a concomitant increase, to 42%, in the amount that localizes to Vps17-decorated endosomes. Essentially equivalent amounts of Vps10-GFP are accounted for in wild-type and *mvp1*Δ cells (81% and 78%, respectively), with the unaccounted fractions due to threshold limits and localization to compartments that are not decorated by Sec7 or Vps17. These results show that Vps10 is depleted from the Golgi in *mvp1*Δ cells and accumulates in the endosome, and they suggest that Mvp1 has a role in retrograde sorting of Vps10. In further support of functional links between Mvp1 and retromer, cluster analyses of genome-scale

Downloaded from jcb.rupress.org on June 24, 2015

Published February 24, 2014

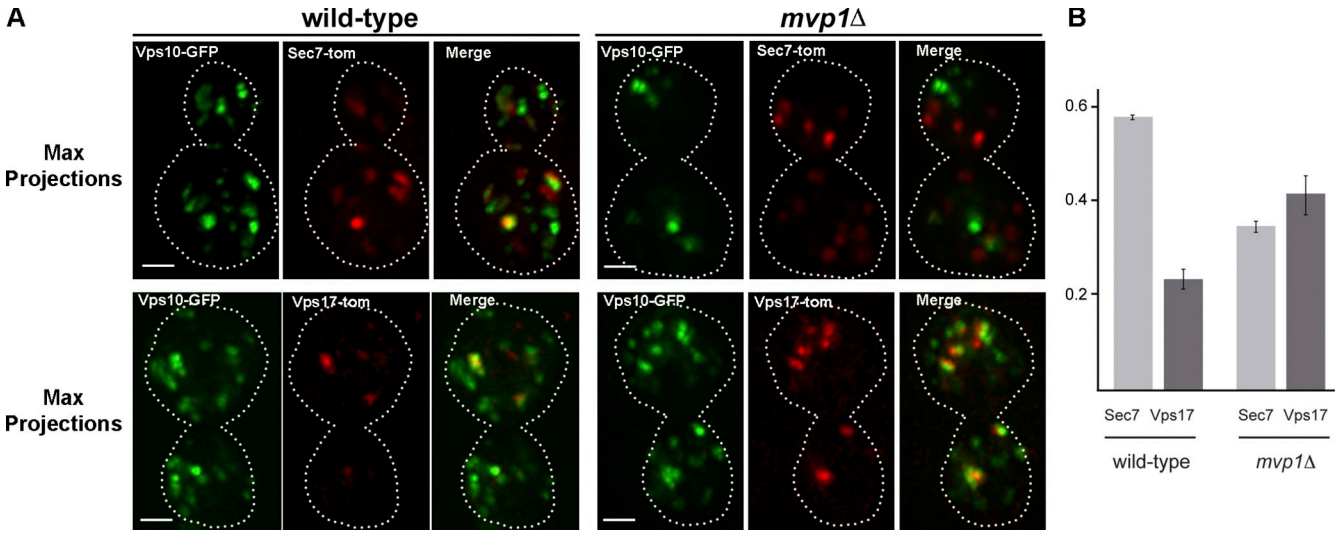

Figure 1. **The Vps10 sorting receptor accumulates in retromer-decorated endosomes in *mvp1*Δ-null mutant cells.** (A) Micrographs showing Vps10 (Vps10-GFP) coexpressed with either Sec7-tomato (Sec7-tom) or Vps17-tomato in wild-type and *mvp1* Δ cells are shown. Bar, 1 µm. (B) Distribution of Vps10-GFP between the Golgi and endosome in wild-type and *mvp1*Δ cells. The proportion of Vps10-GFP that localizes to Golgi compartments decorated by Sec7-tomato and endosomes decorated by Vps17-tomato in wild-type and *mvp1*Δ cells is shown.

S. cerevisiae and *Schizosaccharomyces pombe* genetic profiling datasets show that the genetic interactions of *mvp1*Δ and retromer-null mutants are closely correlated (Costanzo et al., 2010; Koh et al., 2010; Frost et al., 2012).

Mvp1 and retromer SNX-BARs decorate a tubular endosomal network

Endosomes in yeast cells typically appear as punctate objects when visualized by wide-field epifluorescence microscopy of endosomal proteins, and no dynamic domain, akin to the TEN in mammalian cells, has been described. Given the fundamental role of the TEN in cargo sorting, and the evolutionary conservation in structure and function of SNX-BAR proteins, we examined structural features of endosomes decorated by GFP-tagged Mvp1 and Vps17 SNX-BARs and the Vps26 retromer subunit using time-lapse fluorescence microscopy. Images of a single focal plane within cells were acquired at 270-ms intervals, which allowed us to monitor an endosome for up to 10 s before bleaching of the GFP signal. Successive images (Fig. 2 A, Fig. 3) reveal Mvp1-GFP– and Vps17-GFP–decorated endosomes to be structurally dynamic organelles where each protein decorates a punctate, presumably vacuolar, structure and a physically associated tubular network that has not been previously described for yeast endosomes. Coated tubules and vesicles emerge from a mother endosome, undergo fission, and then move away from the endosome. Tubule budding/fission cycles were completed within 540–810 ms and yielded tubules that we estimate to be ∼150–200 nm in length, though this could not be precisely determined because of the diffraction limit. There was substantial heterogeneity in the dynamics of individual endosomes; a tubular network was not observed to be associated with every SNX-BAR–coated endosome during the time window of these experiments, and we observed, though infrequently, entire SNX-BAR–coated endosomes to convert into an interconnected tubular network and then fragment (Video 1). The fluorescence intensity of budding endosomes decreased over time, whereas the intensity of inactive endosomes did not decrease as rapidly, allowing us to discern that the dynamic features of these organelles and the loss of SNX-BAR signal from active endosomes was not due to photobleaching. Finally, we also observed apparent homotypic exchanges between endosomes in which a budding tubule appeared to undergo fission and then fuse with a nearby endosome (Video 1). The small sizes, short lifetimes, rapid movements, and low SNX-BAR fluorescence signal of these tubules may explain why they have not been described previously.

Purified recombinant human SNX8 and retromer SNX-BARs (SNX1 and SNX5) do not form higher order oligomers in vitro and have been proposed to coat distinct transport carriers (van Weering et al., 2012a). Hence, it was of interest to test if yeast Mvp1 and retromer SNX-BARs decorate the same, or distinct, endosome-derived tubules in vivo. To do so, we used time-lapse fluorescence microscopy to examine Mvp1-2xRFP and Vps17-GFP (Fig. 2, B and C) in the same cell. Because of the dynamic nature of the TEN and that mRFP is not as bright as, and bleaches more rapidly than, GFP, we fused a tandem 2xmRFP tag to query proteins and captured three successive SNX-BAR-GFP frames at 50-ms intervals for each 2xmRFP frame (200-ms exposure). Successive GFP images were overlayed and compared side-by-side to the 2xmRFP image (Fig. 2, B–D). We observed that 54% of the tubules that are decorated by Vps17-GFP are also decorated by Mvp1-2xmRFP, although there is a substantial proportion of tubules that contain either Vps17-GFP or Mvp1-2xmRFP, but not both (33% and 13%, respectively). Because these results indicate that endosome-derived tubules possess a mixed coat of retromer and Mvp1 SNX-BARs, we tested for physical interactions between Mvp1 and retromer subunits (Vps5, Vps17, Vps35), but found no evidence that Mvp1 forms heterodimers with Vps5 or Vps17, or that Mvp1 associates with retromer trimer, or that it recognizes the Vps10 cargo protein. These results are in line with a recent study showing that human SNX8 and the

Downloaded from jcb.rupress.org on June 24, 2015

Published February 24, 2014

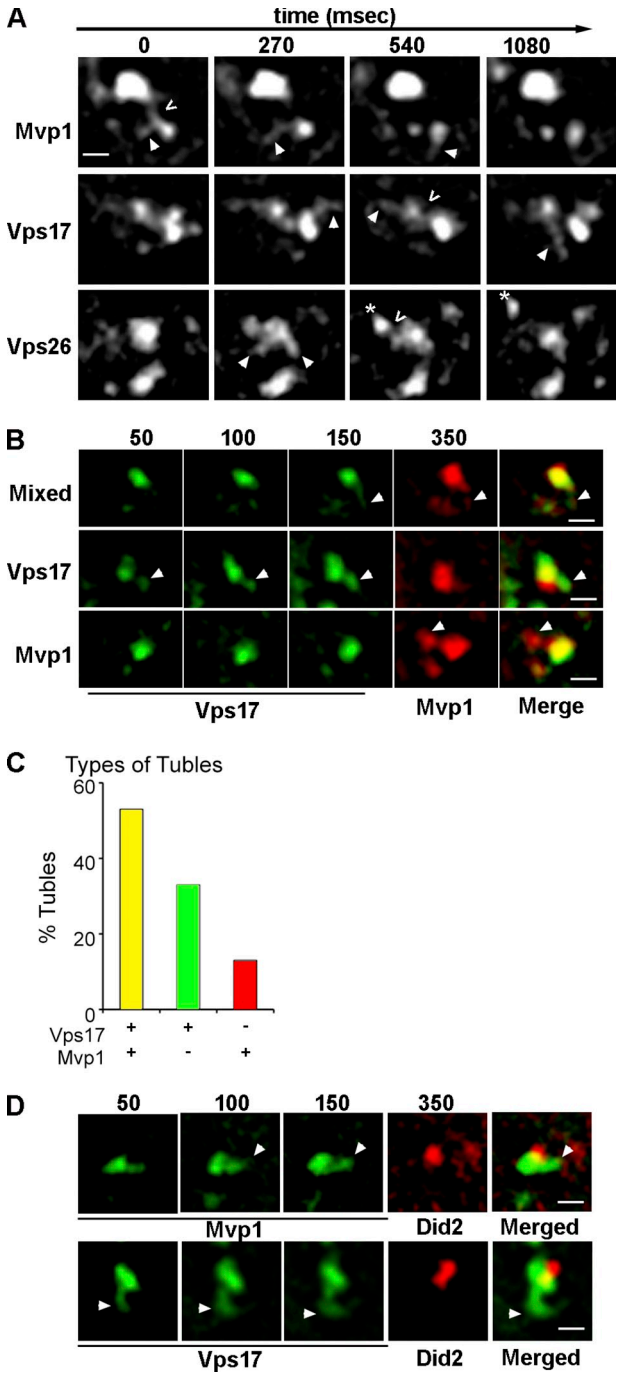

Figure 2. **Mvp1 and Vps17 retromer SNX-BAR coat tubules that bud from the endosome.** (A) Micrographs of Mvp1-GFP–, Vps17-GFP–, or Vps26-GFP–decorated endosomes captured by time-lapse fluorescence deconvolution microscopy. Arrowheads point to a tubule of interest and open arrows (<) indicate a presumptive fission event. Images were captured at a single focal plane within cells and acquired at 270-ms intervals. (B) Micrographs showing tubules emanating from Vps17-GFP– and Mvp1-2xmRFP–decorated endosomes were captured by time-lapse fluorescence microscopy. An example of a tubule decorated by both Vps17-GFP and Mvp1-2xmRFP ("Mixed") is shown on the top, a tubule decorated only by Vps17-GFP in the middle, and a tubule decorated by only Mvp1-GFP on the bottom. (C) Quantitation of the different types of SNX-BAR–coated tubules. (D) Micrographs showing Vps17-GFP–coated (top) or Mvp1-GFP– coated (bottom) tubules emanating from an endosome also decorated by Did2-mKate2. Image capture speeds for each strain was 50 ms for the GFP channel and 200 ms for the RFP channel. Bar, 500 nm.

retromer SNX-BARs, SNX1 and SNX5, do not co-immunopurify from cell extracts and do not hetero-oligomerize in vitro (van Weering et al., 2012a).

Several features of the SNX-BAR–coated TEN were examined to determine if it has a role in retromer-mediated sorting. First, we considered the possibility that apparent fission events correspond to whole organelle fission rather than the biogenesis of bona fide transport carriers. To address this, we tested if a component of the multivesicular body (MVB)–sorting pathway, Did2 (expressed as a functional mKate2 C-terminal fusion) could be observed on SNX-BAR–coated tubules. Although Did2-mKate2 localizes with a subset of Mvp1-GFP– and Vps17-GFP–decorated endosomes, it was never observed on budding SNX-BAR–coated tubules. Moreover, we observed a striking juxtaposition of Did2-mKate2 to a SNX-BAR-GFP domain from where a tubule emerged (Fig. 2 D). The signals of Mvp1-GFP and Vps17-GFP were observed to overlap that of Did2 only minimally, consistent with these components of the retrograde sorting and degradative sorting machineries segregating into distinct domains on the endosome. This result indicates that the SNX-BAR–coated domain of the endosome, but not the ESCRT-coated domain that sorts cargo into the degradative pathway, is active in budding of tubules.

Next, we determined if a retromer cargo, Vps10, could be detected in budding tubules/vesicles. Vps10 was tagged with 2xmRFP in cells expressing GFP-tagged Mvp1 or Vps17 and the proportions of SNX-BAR–coated tubules containing Vps10-2xmRFP were determined. Of 30 tubules scored, Vps10 was present in 60% of Mvp1-decorated tubules and 50% of Vps17-decorated tubules (Fig. 3, A–C). We also observed Mvp1- and Vps17-coated tubules that lacked Vps10-2xmRFP (14% and 30%, respectively) and tubules containing Vps10, but not Mvp1 or Vps17 (26% and 20%, respectively). Importantly, Vps10-containing tubules were not observed to be decorated by Did2, a protein which functions in the ESCRT-mediated degradative pathway (Fig. 3 A, bottom). These observations lead us to conclude that a substantial fraction Vps17-coated tubules (conservatively estimated to be at least 50%) and Mvp1-coated tubules (at least 60%) constitute retrograde carriers, and that at least 50% of these carriers are coated by both Vps17 and Mvp1. To determine if Mvp1 is required to bud retromer SNX-BAR–coated tubules, we determined the budding frequency, defined as the number of tubule-budding events observed from a single endosome in 10 s, for Vps17-GFP–coated tubules in cells lacking Mvp1 (Fig. 7 D). This analysis showed that budding frequency trends greater in *mvp1*Δ cells, though the difference is not statistically significant. Hence, the formation of retromer SNX-BAR–coated tubules does not require Mvp1 and the basis of the Vps10 endosome export defect of *mvp1*Δ cells (Fig. 1) is not explained by a defect in the formation of the TEN.

Mvp1 possesses potent in vitro membrane remodeling activity

Many SNX-BARs, including the human orthologue of Mvp1, SNX8, can remodel membrane vesicles into tubules, and this has been proposed to underpin their functions in endosomal sorting and cargo export (van Weering et al., 2012a). We tested

Downloaded from jcb.rupress.org on June 24, 2015

Published February 24, 2014

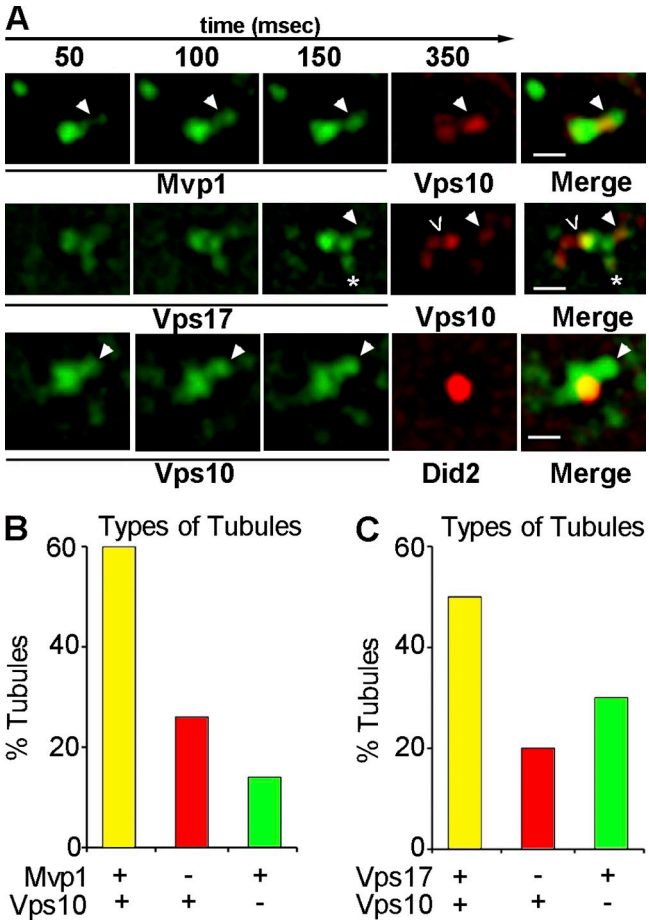

Figure 3. **Retromer- and Mvp1-coated SNX-BAR–coated tubules contain retrograde cargo.** (A) Galleries of representative time-lapse micrographs showing endosomes from cells coexpressing Vps10-2xmRFP and either Mvp1-GFP or Vps17-GFP and cells coexpressing Vps10-2xGFP with Did2-mKate2. A single tubule colocalized for both Mvp1 and Vps10 is shown in the top row. The middle row shows a Vps17-mGFP–decorated endosome and three types of tubules; a tubule decorated by both Vps17-GFP and Vps10-2xmRFP (filled arrowhead), a tubule containing Vps10-2xmRFP but not Mvp1-GFP (<), and a tubule containing Vps10-2xmRFP but not Vps17-GFP (*). The bottom row shows time-lapse micrographs of a Did2-mKate2 endosome from which a tubule containing Vps10-GFP, but not decorated by Did2-mKate2, is budding (arrowhead). The end point (milliseconds) of each exposure is indicated on the top. Bar, 500 nm. (B) The proportion of tubules decorated by Vps17-GFP and containing Vps10-2xmRFP in wild-type and *mvp1*Δ cells is plotted. (C) The proportion of tubules in cells expressing Mvp1-GFP and Vps10-2xmRFP is plotted.

membrane remodeling activity of Mvp1 by incubating full-length, recombinant Mvp1 with liposomes containing PtdIns3*P* prepared by extrusion through a 200-nm filter and examining the products by negative-stain electron microscopy. Membrane tubules were observed in reactions containing 10 µM and 20 µM Mvp1, but not in reactions without Mvp1 (Fig. 4 A); however, there were two unexpected features of the reactions. At both concentrations of Mvp1, the most striking and abundant products were coated vesicles (Fig. 4 A). Whereas a broad size distribution of vesicles with an average diameter of 171.6 ± 96.8 nm was observed in reactions without Mvp1, uniformly sized vesicles of an average diameter of 54.4 ± 12.3 nm were observed in the presence of Mvp1 (Fig. 4, B and C). Further, the abundance of the vesicles is positively correlated with the amount of Mvp1 in the reaction, and is inversely correlated with the abundance of tubules, indicating that vesicles are formed from tubules by fission. Consistent with this, the diameter of tubules in the 20-µM Mvp1 reaction is 35.8 ± 18.2 nm ($n = 9$), and is 63.3 ± 15.3 nm ($n = 29$) in the 10 µM Mvp1 reaction ($P < 0.0001$; Fig. 4 D), suggesting that Mvp1 may have multiple packing modes on a membrane. Fission activity has been observed for the BAR proteins endophilin and amphiphysin (Peter et al., 2004; Gallop et al., 2006; Boucrot et al., 2012), but to our knowledge, has not previously been reported for a SNX-BAR protein.

The dynamin-related protein, Vps1, is required for endosomal retrograde trafficking

The *MVP1* gene was first identified by its activity as a multicopy suppressor of the vacuolar protein sorting defect of cells expressing a dominant-negative *VPS1* allele (*vps1*^{d}; Ekena and Stevens, 1995). The genetic relationship between *MVP1* and *VPS1* prompted us to consider a role for Vps1 in retrograde transport from the endosome. To first address this, we examined localization of Vps1-GFP in wild-type haploid cells that co-express mCherry-Ypt7, a marker of late endosomes and the vacuole, and observed that Vps1-GFP localizes to large puncta that are not decorated by mCherry-Ypt7 or other markers of the endosomal system (Fig. S2). The vacuoles in these cells are severely fragmented and the cells secrete as much vacuolar CPY as *vps1*Δ cells, both hallmarks of *vps1*Δ cells (Raymond et al., 1992), suggesting that Vps1-GFP is not fully functional. Because dynamin family proteins function as oligomers, we examined Vps1-GFP in diploid strains carrying one untagged and one GFP-tagged *VPS1* allele. Strikingly, normal vacuole morphology is restored in these cells and Vps1-GFP localizes to 5–10 small puncta, many of which appear tethered to the vacuole (Fig. 5; Fig. S2). Many Vps1-GFP–positive puncta are also decorated by Mvp1-2xmRFP, Vps17-2xmRFP, and Did2-mKate2, identifying them as endosomes (Fig. 5; Fig. S2). Endosome localization of Vps1-GFP is strongly influenced by the presence of Mvp1, as there is a dramatic reduction in endosome localized Vps1-GFP in cells lacking Mvp1 (i.e., *mvp1*Δ *mvp1*Δ *VPS1 VPS1-GFP*). To quantify the contribution of Mvp1 to endosome targeting of Vps1-GFP, we determined the proportion of Vps17-2xRFP, Vps1-GFP double-positive endosomes (Fig. 5 B). As cells typically contain 3–5 endosomes decorated by Vps17-2xRFP, cells were binned in quartiles (with an additional "zero" class). Although for the wild-type strain, 60% of cells are in the 75–100% double-positive class, in *mvp1*Δ *mvp1*Δ cells there are none in this class and the peak of the distribution (representing 55% of the cells) is the 26–50% double-positive class. In wild-type cells, of all Vps17-positive endosomes examined, Vps1-GFP is detected on 82% of them, but only 34% of endosomes in *mvp1*Δ *mvp1*Δ cells contain detectable Vps1-GFP (Fig. 5 C). Similar results were obtained when we compared a different endosome marker, Did2-mKate (Fig. S2). These data indicate that Vps1 localizes to the endosome via an indirect mechanism that is promoted by, but is not entirely dependent upon, Mvp1.

Downloaded from jcb.rupress.org on June 24, 2015

Published February 24, 2014

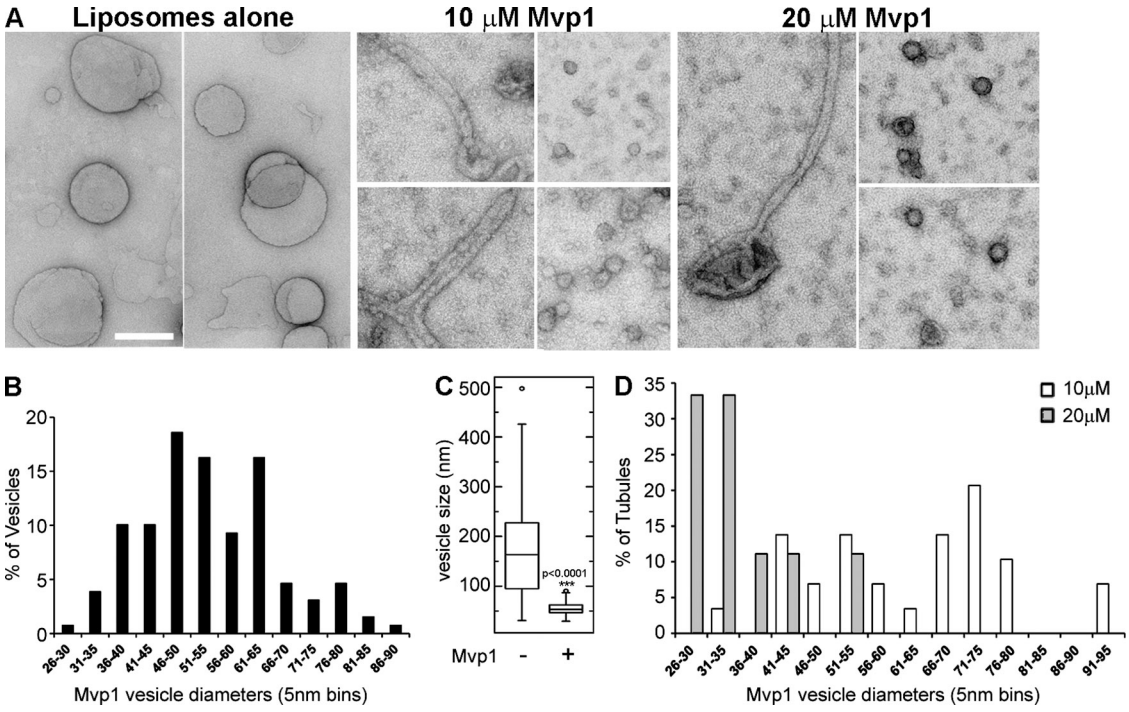

Figure 4. **Mvp1 possesses potent membrane remodeling activity.** (A) Gallery of micrographs of negative-stained liposomes incubated with SNX-BAR Mvp1 at indicated concentrations. Bar, 200 nm. Montages of micrographs for each condition showing representative vesicles or tubules generated by Mvp1 are shown. (B) Histogram of the diameter of vesicles generated by Mvp1 (n = 129 vesicles) in 5-nm bins. (C) Box-plot compares the distribution of vesicle diameters generated by Mvp1. Average vesicle diameters of liposomes alone are 171.6 ± 96.8 nm, n = 55, and with Mvp1 are 54.4 ± 12.3 nm, P < 0.0001 (unpaired t test). (D) Histogram of the diameter of tubules generated by 10 or 20 µM Mvp1 in 5-nm bins. 10 µM Mvp1 (n = 29) generated average tubule diameters of 63.3 ± 15.3 nm, and 20 µM Mvp1 (n = 9) generated average tubule diameters of 35.8 ± 18.2 nm, P < 0.0001 (unpaired t test).

To probe for a role for Vps1 in the endosomal system, we first examined the structures and dynamics of endosomes in *vps1*Δ cells using fluorescence and electron microscopy (Fig. 6). Quantitation of fluorescence micrographs of SNX-BAR (Mvp1, Vps17) and retromer (Vps26) proteins reveals ∼1.5-fold increases in the average number of endosomes per cell and average endosome size in *vps1*Δ cells compared with wild-type cells (Fig. 6 B). In contrast, the average number of Sec7-GFP–decorated Golgi compartments is unchanged (Fig. 6 B). We also observed that the fluorescence intensity of retromer (i.e., Vps26-GFP) signal on endosomes of *vps1*Δ cells is increased approximately twofold, indicating that retromer accumulates on these endosomes (unpublished data). Thin-section (90 nm) electron microscopy of *vps1Δ* cells confirmed the increased diameters of MVBs (149.4 nm ± 9.793, n = 11; 193.5 nm ± 7.267, n = 28; P = 0.018 wild-type vs. mutant, respectively; Fig. 6, D–H).

These results clearly show that loss of Vps1 has a profound impact on the morphology of endosomes, and to directly address a role for Vps1 in the retromer pathway we examined Vps10-2xGFP in *vps1*Δ cells. Whereas in wild-type cells Vps10-2xGFP localizes to punctate Golgi and endosome compartments, in *vps1*Δ cells Vps10-2xGFP localizes prominently to the vacuole membrane (Fig. 6 C), a localization that phenocopies retromer-deficient cells (Liu et al., 2012). Consistent with vacuole localization of Vps10, the subcellular fractionation profile of Vps10-myc in *vps1*Δ cells shows a shift to the vacuole-enriched P13 fraction and the appearance of degradative intermediates, as observed with a retromer-null (*vps35Δ*) strain (Fig. 7 A; Luo and Chang, 2000), and similar to the fractionation profile of Kex2, another retromer cargo (Wilsbach and Payne, 1993). Together with earlier reports showing a defect in Snc1 trafficking in *vps1*Δ cells (Burston et al., 2009; Smaczynska-de Rooij et al., 2012), the results strongly support a role for Vps1 in the endosome-to-Golgi retrograde pathway.

An expanded tubular endosomal network in *vps1*Δ cells

In consideration of the general role of dynamin family proteins in membrane fission and the retrograde-sorting defects of *vps1*Δ cells, we speculate that Vps1 provokes fission of SNX-BAR–coated tubules from the endosome, and to test this we used time-lapse fluorescence microscopy to compare the dynamics of SNX-BAR–coated endosomes in *vps1*Δ and wild-type cells. The results of several experiments support this hypothesis. Subcellular fractionation experiments show that the distribution of myc epitope-tagged Vps10 is shifted to the vacuole containing the 13,000 *g* fraction, and degradative products are observed, to a similar extent as retromer-null (i.e., *vps35*Δ) cells (Fig. 7 A). In contrast, in *mvp1*Δ cells Vps10 is relatively stable and its distribution between the P13 and P100 fractions is unaltered compared with wild-type cells, as expected from the Vps10 fluorescence data (Fig. 1).

When we examined SNX-BARs in *vps1*Δ cells, we observed an expanded TEN in which tubules emerged and then often retracted into the mother endosome (Fig. 7 B), similar to endocytic plasma membrane retraction events observed in *vps1*Δ

Downloaded from jcb.rupress.org on June 24, 2015

Published February 24, 2014

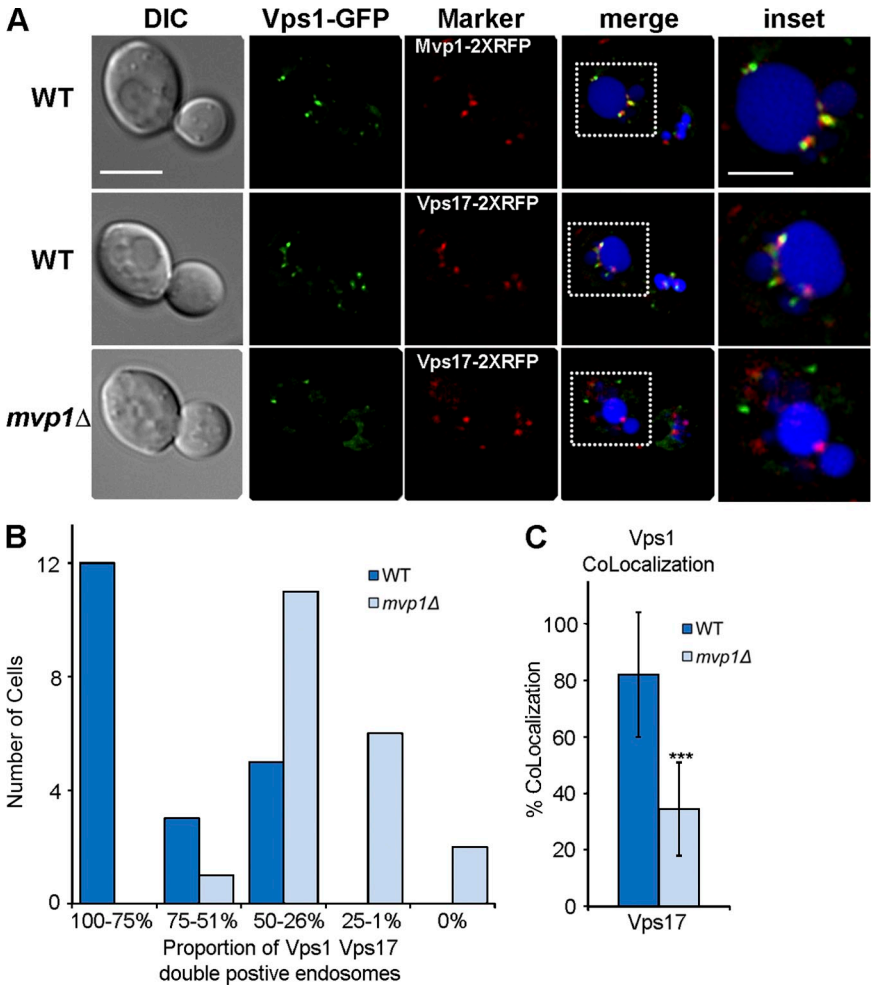

Figure 5. **Vps1 dynamin family protein localizes to SNX-BAR–coated endosomes.** The top row shows diploid cells expressing one untagged copy of Vps1 and one GFP-tagged copy of Vps1 (Vps1-GFP) in cells coexpressing Mvp1-2xRFP (top) or Vps17-2xRFP (middle). Vacuoles (blue) were visualized by staining with the vital dye, CMAC. An expanded view of the boxed region in the "merge" column is shown in the "inset" column. The bottom row shows Vps1-GFP in homozygous diploid *mvp1*Δ *mvp1*Δ cells. One deconvolved image of a z-series containing the endosome or vacuole marker is shown. Bar: (main panels) 5 µm; (insets) 2.5 µm. Two methods for representing colocalization of Vps1-GFP with Vps17-2xRFP are depicted in B and C. Refer to text for a detailed description of the quantitation methods. (B) Distribution of the proportion of Vps1-GFP and Vps17-2xRFP double-positive endosomes. Wild-type (dark blue) and *mvp1*Δ *mvp1*Δ (light blue) cells (n = 20) were binned according to the proportion of Vps1-GFP and Vps17-2xRFP double-positive endosomes. (C) The proportion of endosomes (wild type: n = 64 of endosomes; *mvp1*Δ: n = 82 endosomes derived from cells analyzed in B) decorated by both Vps1-GFP and Vps17-2xRFP are shown. Standard deviations are indicated; $P < 0.0001$ (unpaired t test).

cells (Smaczynska-de Rooij et al., 2010). Due to the irregular shape of these tubules, it was not possible to accurately measure their sizes, but because they grow larger over time, we defined a surrogate parameter, "tubule lifetime," as the time interval between the first frame when a tubule emerges from the mother endosome and the frame when the tubule retracts into the mother endosome or when a discontinuity between the tubule and mother endosome is observed. In wild-type cells, Mvp1 and Vps17 tubule lifetimes ranged from 270 to 1600 ms, with an average of 570 ± 407 ms and 457 ± 188 ms, respectively (Fig. 7 C). In *vps1*Δ cells, Mvp1- and Vps17-coated tubule lifetimes are increased two- to threefold, ranging from 270 to 3254 ms, with an average of 1348.3 ± 693 ms and 856.5 ± 560 ms, respectively (Fig. 7 C). These data are consistent with a role for Vps1 in fission of SNX-BAR–coated tubules.

Tomographic models of *vps1*Δ cells also revealed profound changes in the appearance of endosomes, including visually striking examples of endosomal tubules, ∼50 nm in diameter and variable in length, that are rarely observed in wild-type cells (Fig. 8; Video 2). These tubular networks contain very few ILVs, suggesting these are early endosomes that are actively sorting cargo, in contrast to the large number of ILVs within mature MVBs/late endosomes that most likely represent the subset of endosomes that we describe as inactive in tubule budding. The MVBs of *vps1*Δ cells possess fewer ILVs than wild-type cells (wild-type: 38.58 ILVs ± 5.984, n = 12; *vps1*Δ: 17.83 ILVs ± 3.154, n = 18; unpaired t test, $P = 0.0024$), resulting in a reduction in proportional ILV surface area per MVB (wild type: MVB = 47.62%, ILV = 52.38%; *vps1*Δ: MVB = 65.78%, ILV = 34.22%; Fig. 8 E). Surprisingly, the average size of MVB ILVs is increased (25.55 nm ± 0.2307; 30.65 nm ± 0.9362; n = 102, $P < 0.0001$ wild-type vs. mutant, respectively; Fig. 8 D) and the mean number of ILVs per MVB is reduced. Finally, we observed in *vps1*Δ cells apparently tethered cisternae resembling the aberrant endosomes that accumulate in ESCRT mutants (the "class E compartment"; Fig. 8, A–C).

Discussion

Mvp1 is a component of the retromer pathway

The data presented here show that Mvp1 functions with retromer to evoke endosome-to-TGN trafficking of retrograde cargo, revealing a previously unappreciated link between Mvp1 and retromer. This finding was unexpected as SNX8, the human homologue of Mvp1, was proposed to be a component of a retromer-independent endosome-to-TGN pathway (Dyve et al., 2009). However, this conclusion was based on the opposite

Downloaded from jcb.rupress.org on June 24, 2015

Published February 24, 2014

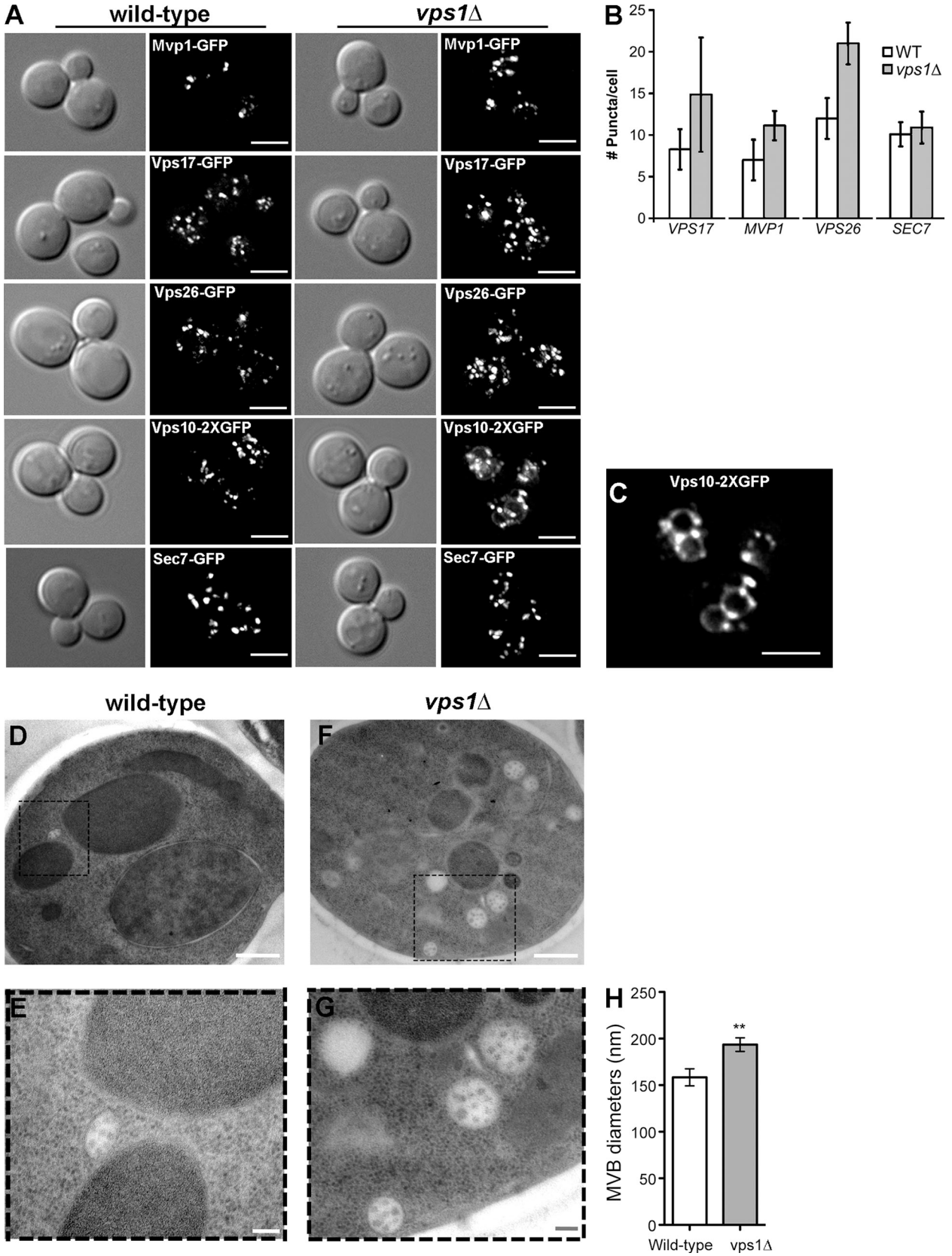

Figure 6. **Loss of Vps1 dynamin family GTPase impacts endosome number and morphology.** (A) The indicated GFP-tagged endosomal proteins and Vps10 were visualized in wild-type and *vps1*Δ cells. Maximum projections of deconvolved z-stacks are shown. Bar, 5 µm. (B) Quantitation of SNX-BAR–, retromer-, and Sec7-decorated (Golgi) compartments in wild-type and *vps1*Δ cells. The number of puncta per cell was determined by masking each new punctum in each z-section. The average number of puncta per cell, wild-type vs. *vps1*Δ, and standard deviation, is shown for each of the indicated proteins. Every endosome marker showed significantly more puncta per cell: Vps17, 8.2 ± 2.4 vs. 14.8 ± 6.8; Mvp1, 7 ± 2.5 vs 11.1 ± 1.7; Vps26, 12 ± 2.5 vs. 21 ± 2.5;

Downloaded from jcb.rupress.org on June 24, 2015

Published February 24, 2014

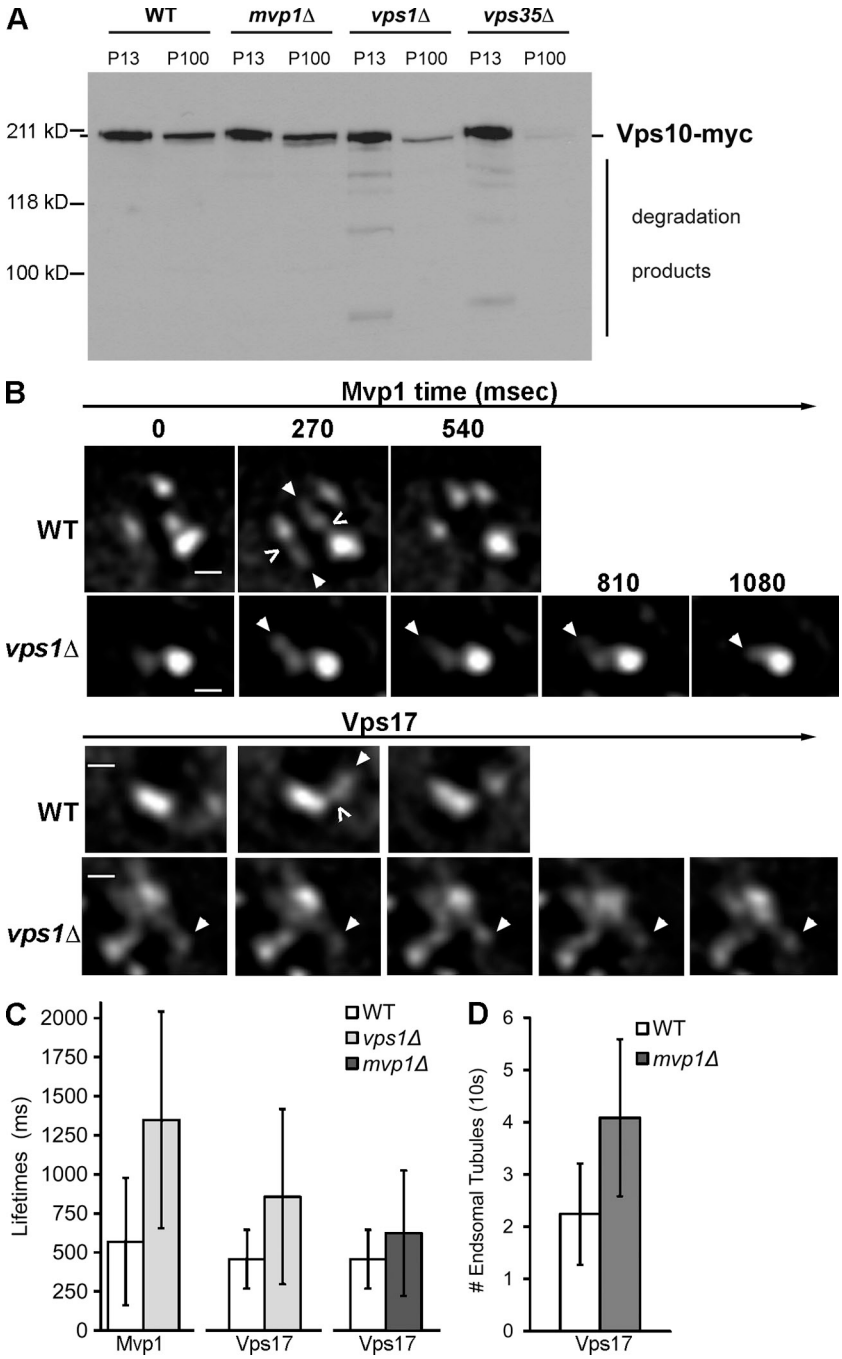

Figure 7. **Loss of Vps1 dynamin family GTPase results in deficient fission of SNX-BAR–coated tubules.** (A) Subcellular fractionation analysis of Vps10-myc. Spheroplasts derived from the indicated strains were lysed and a low-speed membrane pellet (13,000 *g*) and a high-speed membrane pellet (100,000 *g*) were generated. Equivalent amounts of each fraction were separated by SDS-PAGE and immunoblotted with anti-myc antibody. The position of full-length Vps10-myc is indicated, as well as degradative products that arise as a result of proteolysis by vacuolar proteases. The positions of molecular mass (kD) markers are indicated. (B) Time-lapse gallery of Mvp1-GFP– and Vps17-coated endosomes in wild-type and *vps1*Δ cells by time-lapse fluorescence deconvolution microscopy. Arrows highlight a tubule of interest in each time-lapse series and open arrow (<) indicates a fission event. (C) Tubule lifetimes were calculated as described in the text for Mvp1-GFP– or Vps17-GFP–coated tubules. Vps17 tubule lifetimes were significantly increased in *vps1*Δ cells ($P = 0.0005$) and in *mvp1*Δ cells ($P = 0.043$). (D) Vps17 tubule frequencies were calculated as described in the text. The frequency of Vps17-GFP tubules increased approximately twofold in *mvp1*Δ cells ($P < 0.0001$).

effects of RNAi-mediated depletion of SNX8 and VPS35 on trafficking of an exogenous cargo, Shiga toxin, and to date, no endogenous SNX8-specific cargos have been described. We have examined sorting of many different yeast plasma membrane and TGN proteins in *mvp1*Δ and retromer-null cells but have not identified any cargo whose steady-state localization is affected by loss of Mvp1, but not retromer. Thus, Mvp1 can be considered a component of the retromer-mediated retrograde pathway.

Neither we, nor others (van Weering et al., 2012a), have uncovered any biochemical evidence that Mvp1 or SNX8 functions with retromer as a "super complex." How might Mvp1 influence retromer function without directly associating with it? Current models of SNX-BAR membrane coats emphasize their abilities

Sec7 (Golgi), 10.1 ± 1.4 vs. 10.9 ± 1.9; $n = 30$ for each strain, $P < 0.0001$ (unpaired *t* test), wild-type and *vps1*Δ, respectively. (C) To better visualize vacuole localization of Vps10 in *vps1*Δ cells, a single plane of the z-section containing vacuoles from the maximum projection shown in A is shown. Bar, 5 µm. (D and E) Thin-section electron micrographs of multivesicular endosomes in wild-type and *vps1*Δ cells (F and G) with endosomes highlighted in reference images at low magnification (D and F; bar, 500 nm) and shown at high magnification (E and G; bar, 100 nm). (H) Multivesicular bodies in *vps1*Δ cells are larger than in wild-type cells (unpaired *t* test, $P = 0.0084$; *vps1*Δ 193.5 nm ± 7.267, $n = 28$; wild-type 158.3 nm ± 9.179, $n = 12$).

Downloaded from jcb.rupress.org on June 24, 2015

Published February 24, 2014

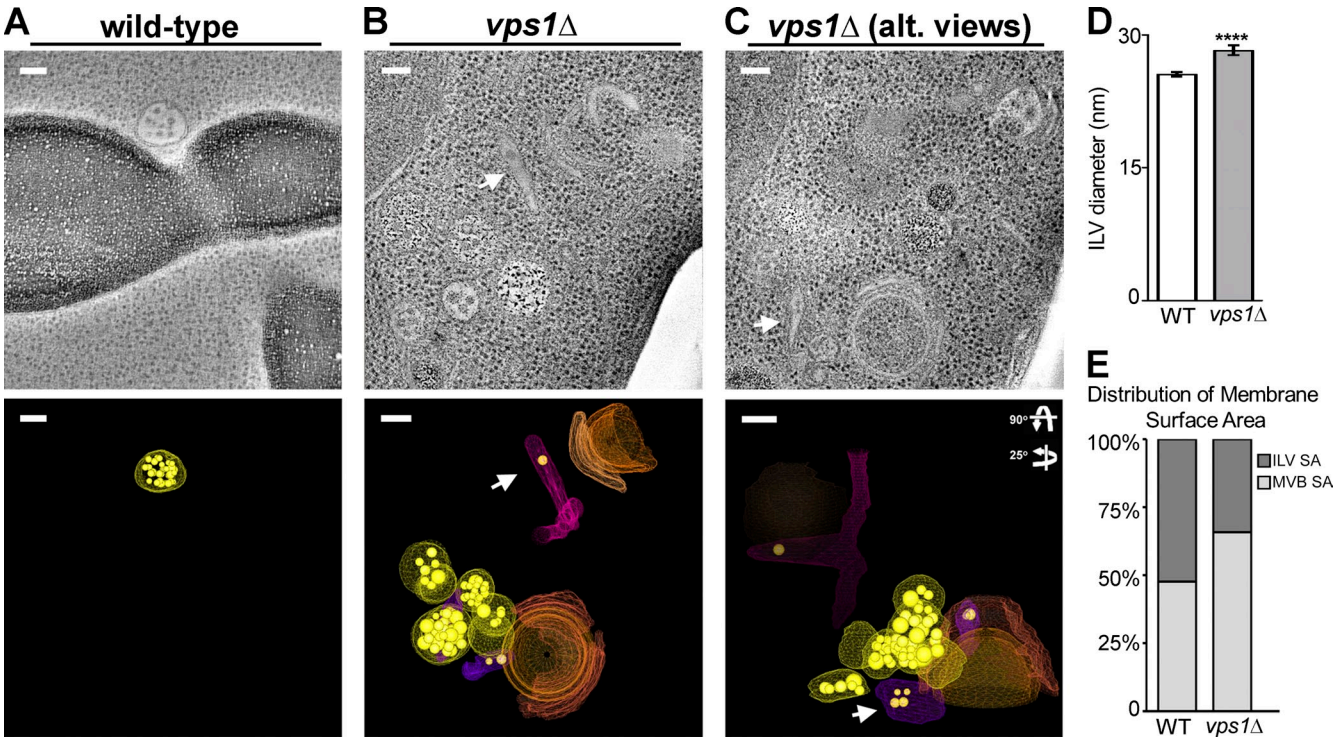

Figure 8. **Tomographic representations of *vps1Δ* cells reveal aberrant endosome morphology.** (A and B) Multivesicular bodies observed by electron tomography (ET) are spherical (A and B, yellow models, $n = 7$; average diameter = 131 nm, similar to wild-type) and tubular (B and C, arrows and purple models, $n = 3$; average diameter, ~50-nm diameter, variable length). Spherical MVBs observed by ET are smaller than those observed by thin-section EM quantitation. Small cisternal endosomes are also observed associated with endosomes (B and C, orange models). Tubular endosomes had fewer ILVs and were associated with other endosomes or vacuoles (B and C). (D) Intraluminal vesicle diameters from *vps1Δ* cells are significantly larger than wild-type (unpaired *t* test, P = 0.0001; wild type 25.55 nm ± 0.2307, $n = 333$; *vps1Δ* 30.65 nm ± 0.9362, $n = 102$). (E) Multivesicular bodies in *vps1Δ* cells have increased limiting membrane surface area and decreased ILV surface area compared with MVBs in wild-type cells. The distribution of endosomal membrane and internalized intraluminal vesicle membrane in wild-type and *vps1Δ* cells are plotted. In wild-type cells the surface areas of MVB and ILV are nearly equal (paired *t* test, P = 0.7434). In *vps1Δ* cells there is a loss in ILV surface area compared with the MVB surface area (paired *t* test, P = 0.0002). The mean ILV surface area generated in *vps1Δ* cells compared with wild-type (unpaired *t* test, P = 0.0049; wild-type 58924 ± 8591 nm^2, $n = 12$; *vps1Δ* 27751 ± 6069 nm^2, $n = 20$). The mean surface areas of endosomal limiting membrane of wild-type and *vps1Δ* cells were not significantly different (unpaired *t* test, P = 0.947; wild-type 57034 ± 6607 nm^2, $n = 12$; *vps1Δ* 57690 ± 6459 nm^2, $n = 20$).

to oligomerize into homogeneous lattices that can drive membrane remodeling in vitro (van Weering et al., 2012a); however, it is important to bear in mind that the SNX-BAR coat structures observed in vitro are generated using super-physiological concentrations of purified proteins and that similar structures that have not been described on the TEN in vivo (Carlton et al., 2004; Mari et al., 2008). Our findings suggest that physiological SNX-BAR coats are unlikely to be composed of extensive lattices of a single type of SNX-BAR homo/heterodimer. One implication of this regards the capacity of the TEN to harbor cargo; by first principle, a coat composed of multiple types of protomers (e.g., SNX-BARs) has a higher capacity to accommodate diverse cargo than a coat composed of fewer types of protomers. Thus, the incorporation of Mvp1 into the tubule coat may limit the formation of an extensive regular lattice of retromer SNX-BARs through the formation of Mvp1 oligomers that are incompatible with a retromer-SNX-BAR oligomer (Fig. 9). In this respect, Mvp1 may also provide a kinetic barrier to TEN formation by impeding retromer SNX-BAR oligomerization, which could facilitate cargo surveillance by retromer and subsequent packaging of diverse cargo into the TEN. Consistent with this, RNAi of SNX8 in human cells results in an enhancement of retromer-dependent localization of Shiga toxin to the Golgi (Dyve et al., 2009).

Vps1/dynamin promotes fission of SNX-BAR–coated tubules

Three distinct though not exclusive fission mechanisms for recycling/retrograde carriers have been proposed to operate at the endosomes of mammalian cells, one involving local actin dynamics under regulation by the WASH complex (Derivery et al., 2009; Gomez and Billadeau, 2009; Puthenveedu et al., 2010), a second relying on the AAA family ATPase, spastin (Allison et al., 2013), and a third relying on the GTPase, dynamin (Llorente et al., 1998; Nicoziani et al., 2000; Derivery et al., 2009). The yeast genome does not encode a WASH complex, and our screens for endosomal sorting defects in actin related (e.g., ARP2/3, formin, cdc42, etc.) mutants have not uncovered any deficiencies of endosome function in these mutants, so actin-dependent effects on endosome dynamics are unlikely to play a major role in fission of endosomal tubules, at least in this organism. Similarly, the yeast genome does not encode a spastin orthologue. The results presented here show that Vps1 promotes fission of tubules that emanate from the endosome, contain retrograde cargo, and are coated by retrograde SNX-BARs (Fig. 9). Hence, in contrast to fission events for conventional transport vesicles, multiple distinct mechanisms mediate endosome carrier fission.

Downloaded from jcb.rupress.org on June 24, 2015

Published February 24, 2014

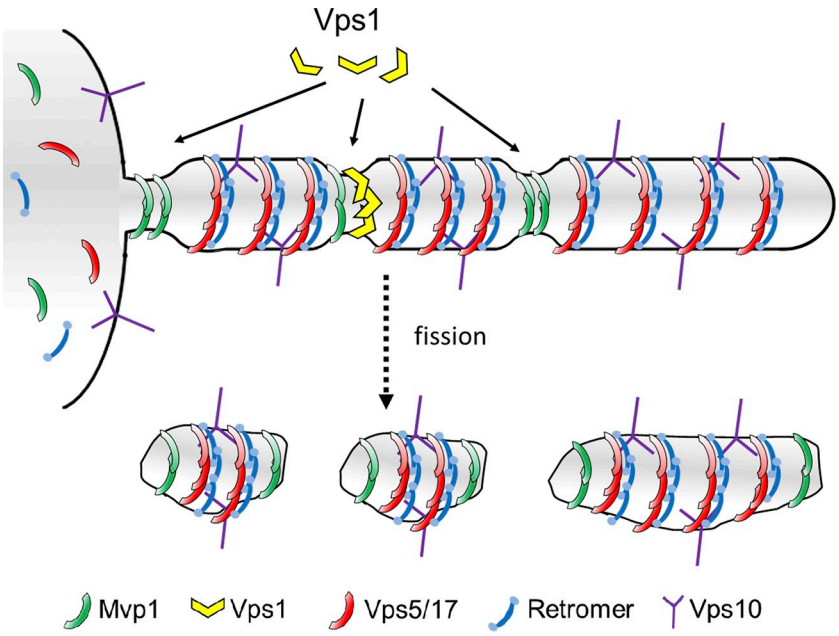

Figure 9. **Mvp1 promotes Vps1-mediated fission of SNX-BAR–coated retrograde carriers from the endosome.** A retrograde tubule budding from an endosome is depicted. The tubule contains integral membrane cargo, Vps10, and is coated by retromer, retromer SNX-BARs (Vps5–Vps17 heterodimer), and Mvp1. Based on the narrow diameter of membrane tubes produced in vitro by human SNX8 (van Weering et al., 2012a), the orthologue of yeast Mvp1, the coated tubule will be constricted at sites where it is wrapped by Mvp1. The constrictions are preferential sites for Vps1 membrane association and oligomerization, leading to fission of the tubule at these sites and the production of retrograde transport carriers of heterogeneous size.

Unexpectedly, we observed widespread and dramatic effects on the endosomal system in cells lacking Vps1. Besides the enlargement of the TEN, there is a pronounced accumulation of MVBs that are larger than MVBs in wild-type cells that are appear to be tethered to each other and the vacuole. Accumulation of these endosomes and flattened endosomal cisternae can be accounted for by the role that Vps1 plays in activating the vacuolar SNARE, Vam3 (Peters et al., 2004; Alpadi et al., 2013; Hayden et al., 2013), and thereby promoting fusion of the late endosome and vacuole. The accumulation of membrane of the limiting membranes of MVBs (approximately twofold increase in surface area) is accounted for in part by the deficiency in membrane export resulting from decreased fission of transport carriers. However, we also observed that MVBs in *vps1*Δ cells possess larger but fewer ILVs, resulting in a substantial decrease in mean ILV surface area per MVB (Fig. 8 E). Perturbations to dynamic ESCRT protein association with the endosome membrane have previously been shown to result in an impairment of cargo sorting and increases in the mean diameters of ILVs and endosome-limiting membranes (Nickerson et al., 2010). Hence, deficient ILV biogenesis is unlikely to reflect a direct role for Vps1 in their formation and we speculate that changes in the endosome membrane composition and tension, as a result of deficient membrane export, impact the MVB pathway.

Vps1 has been proposed to function at numerous organelles, including the retrograde pathway (Deloche and Schekman, 2002; Burston et al., 2009; Smaczynska-de Rooij et al., 2010, 2012), but the mechanisms of intracellular targeting of Vps1 are largely unknown. Canonical dynamins are recruited to sites of endocytosis via direct binding interactions with multiple other components of endocytic machinery, including proteins and lipids (Schmid and McMahon, 2007), but interactions of Vps1 with endosome-localized proteins or lipids has not been reported. Given the genetic relationship between *VPS1* and *MVP1*, we considered it likely that Mvp1 directly binds Vps1 to recruit it to the endosome; however, using a variety of experimental approaches, we have never observed binding of these proteins in solution or on a membrane. How, then, might Vps1 be targeted to SNX-BAR–coated endosomal tubules? Polymerization of pure human dynamin on preformed membrane nanotubes, in the absence of any other proteins, is strongly dependent on the radius of the nanotube, with dynamin nucleation increasing as the radius of the nanotube decreases (Roux et al., 2010). Based on this property, Roux et al. (2010) suggest that, in the range of physiological membrane tension, curvature-promoting proteins elicit dynamin oligomerization on the neck of a budding vesicle. We find that pure Mvp1 can generate membrane tubules of ∼36 nm, which is in close agreement with the average diameter of membrane tubules produced in vitro by pure human SNX8 (∼34 nm; van Weering et al., 2012a). Even more striking, however, is the ability of pure Mvp1 to elicit membrane fission in vitro (Fig. 4), placing Mvp1 in the class of potent membrane-remodeling proteins (Boucrot et al., 2012). With the genetic relationship between Mvp1 and Vps1 (Ekena and Stevens, 1995) in mind, the data provided herein provide compelling evidence that these proteins cooperate to evoke fission of endosomal SNX-BAR–coated tubules in vivo. Intriguingly, Cullen and colleagues found that of all human SNX-BARs tested for tubulation activity, SNX8 generated the narrowest diameter tubules, and that the yeast retromer SNX-BAR, Vps5, generated tubules of ∼50-nm diameter (van Weering et al., 2012a). We show that retromer SNX-BARs and Mvp1 colocalize to a subset of endosome-derived tubules and, hence, these tubules will not be of uniform diameter; Mvp1 oligomers will form constrictions relative to surrounding regions coated with the retromer SNX-BARs (Fig. 9). We suggest that this potentiates Vps1 recruitment to the endosome tubule and, hence, fission of the tubule. Consistent with this, we often observed SNX-BAR–coated tubules to fission into multiple vesicles (e.g., Fig. 2, Vps17-GFP, 1080-ms time point), suggesting that fission occurs at multiple sites along the tubule. Depletion of the endocytic protein Epsin, which can evoke membrane fission on its own, results in deficient dynamin-mediated fission of clathrin-coated vesicles in vivo

Downloaded from jcb.rupress.org on June 24, 2015

Published February 24, 2014

(Boucrot et al., 2012). Thus, membrane-remodeling proteins serve as a common accessory factor for fission executed by dynamin family proteins. Recognition of a "geometric substrate" explains how increased expression of Mvp1 overcomes the deficiency caused by the *vps1*^{d} allele (Ekena and Stevens, 1995); by increasing the area and/or number of high curvature domains on the endosome, Vps1 substrate is increased. Conversely, increased endosome fission can explain the suppression of CPY-sorting defects in *mvp1*Δ cells that overexpress *VPS1*. Importantly, this mechanism also provides Vps1 with the potential to operate on multiple organelles. In summary, our study reveals a close functional cooperation between the endosomal sorting and fission machinery that coordinates the formation of the TEN with the fission of retrograde transport carriers.

Materials and methods

Yeast strains and culture conditions

Yeast strains were constructed in BY4742 (*MAT*α *his3-1, leu2-0, met15-0,* and *ura3-0)*, except the electron microscopy and tomography studies, which used a *vps1*Δ strain constructed in SEY6210 (*MAT*α *leu2-3,112 ura3-52 his3-*Δ*200 trp1-*Δ*901 suc2-*Δ*9 lys2-801; GAL)*. Yeast strains were constructed by integration using recombination of gene-targeted, PCR-generated DNAs using the method of Longtine et al. (1998). Mutant strains used were either derived from the EUROSCARF *KANMX* deletion collection (Open Biosystems/Thermo Fisher Scientific) or produced by replacement of the complete reading frame with the *HIS3MX6* or *URA3* cassette. Gene deletions were confirmed by PCR amplification of the deleted locus. Cells were grown in standard synthetic complete medium lacking nutrients required to maintain selection for auxotrophic markers and/or plasmids (Sherman et al., 1979).

Light microscopy and image analysis

Yeast cells from cultures grown to $OD_{600} \sim 0.5$ were mounted in growth medium, and 3D image stacks were collected at 0.5-µm z-increments on a DeltaVision workstation (Applied Precision) based on an inverted microscope (IX-70; Olympus) using a 100×/1.4 NA oil immersion lens. Images were captured at 24°C with a 12-bit CCD camera (CoolSnap HQ; Photometrics) and deconvolved using the iterative-constrained algorithm and the measured point spread function. Yeast cell cultures were labeled with 7-aminochloromethylcoumarin (CMAC; Molecular Probes) at a concentration of 100 µM for 30 min in synthetic medium at room temperature to examine vacuole morphology. All image analysis and preparation was done using Softworx 5.5 (Applied Precision), unless indicated otherwise.

The analysis of Vps10 distribution shown in Fig. 1 was determined using a manual method implemented using ImageJ v1.38 (National Institutes of Health). A region of interest (ROI) was selected to contain a single cell and the sum of Vps10-GFP fluorescence was calculated. Next, we used the "Mask" macro to delineate the areas within the ROI defined by Sec7-tom and by Vps17-tom. The mask was inverted so that all pixels outside of the mask were assigned a maximum value and the regions corresponding to Sec7-tom or Vps17-tom were assigned a value of zero. Each mask was then overlayed on the Vps10-GFP image and the fluorescence that appeared within the Sec7-tom and Vps17-tom areas was summed and then used to calculate the proportion of Vps10-GFP in each compartment. Minimum thresholds were set manually to minimize the cytosolic signals of each protein and restrict correlation analyses to punctate endosomes, and average correlation coefficients were determined for a minimum of 25 cells in at least three different fields, from at least two different acquisition sessions.

For single-color time-lapse movies, endosomes were focused in a single focal plane in cells expressing endogenously expressed C-terminal GFP fusions. Exposures times of 150 ms resulted in an acquisition time of ∼270 ms per interval, which allowed us monitor an endosome for up to 10 s before photobleaching of the GFP signal. For dual-color time-lapse movies, we captured three successive GFP frames at 50-ms intervals for each 2xmRFP frame (200 ms), leaving the shutter open during acquisition. Movies were then 2D deconvolved using SoftWoRx 5.5 software and successive GFP images were overlayed and compared side-by-side to the 2xmRFP image. Only linear adjustments were made to enhance overall contrast of the tubules and figures were assembled using Adobe Photoshop.

We defined "endosome tubule lifetime" as the time point where a vesicle/tubule emerges from a mother endosome to the time point of either an apparent fission event or the movie frame where the structure completely disappears. Measurements were obtained from single-color time-lapse movies of indicated GFP fusions. Average tubule lifetimes ± SD were determined from 30 tubules for each condition. The Student's *t* test was used to calculate P-values. To determine tubule compositions, endosome tubules were quantified using two-color time-lapse microscopy. The presence of 2xmRFP in the emerging GFP tubule was scored as a mixed/heterogeneous composition. GFP tubules without any 2xmRFP were scored as non-mixed composition. Proportions were obtained from each strain (n = 30). Punctum density (puncta/cell) was calculated using optical z-sections (0.30 µm) of cells (n = 30 for each strain).

Electron microscopy and tomography

Haploid *S. cerevisiae* cells were harvested at log phase, vacuum filtered on 0.45-µm paper (EMD Millipore), loaded into 0.25-mm aluminum planchettes, and high-pressure frozen in a Balzers HPM 010 as described previously (Wemmer et al., 2011). Automated freeze substitution was performed on an AFS system (Leica) with 0.1% uranyl acetate and 0.25% glutaraldehyde in anhydrous acetone, embedded in Lowicryl HM20 (Polysciences, Inc.), and polymerized at −60°C (Giddings, 2003). An ultra-microtome (Leica) was used to cut 90-nm serial thin sections and 250-nm serial semi-thick sections, which were collected onto 1% Formvar films, and adhered to rhodium-plated copper grids (Electron Microscopy Sciences). A transmission electron microscope (CM10; Phillips) was used to image 90-nm sections. Semi-thick sections were labeled with fiduciary 15-nm colloidal gold (British Biocell International) with dual-axis tilt series collected at ±60° with 1° increments using SerialEM (Mastronarde, 2005) at 300 kV, using a microscope (Tecnai F30 FEG; FEI Company). Tilt series were recorded at 29,000× using a 4 × 4-K CCD camera (Gatan, Inc.) with a 0.76-nm pixel as described previously (Wemmer et al., 2011). Individual tomograms were reconstructed using the IMOD package (Kremer et al., 1996) and its newest viewer 3DMOD 4.0.11, and serial tomograms were merged together in x-, y-, and z-direction to obtain a large continuous volume. The 3DMOD modeling software was used for the assignment of the inner leaflet of organelle membrane contours, and IMODINFO was used to obtain surface area and diameter of contour models. We sorted, analyzed, and graphed the data using Microsoft Excel for Mac 2008 and Prism 5 for Mac OS X. Movies were made in 3DMOD and assembled in QuickTime Pro 7.5.

Cell fractionation and immunoblotting

Cell fractionation assays were conducting using a published protocol (Horazdovsky et al., 1994). The anti-myc epitope primary mouse monoclonal antibody used is 9E10 (Covance) and was used diluted 1:5,000. Secondary sheep anti–mouse HRP-conjugated antibody (GE Healthcare) was used at 1:5,000.

Liposome tubulation/vesiculation assays

Liposome tubulation assays were performed as described in van Weering et al. (2012a) with the following modifications. Liposomes were produced from Folch bovine brain lipids (0.5 mg, B1502; Sigma-Aldrich) supplemented with 10 µg synthetic PtdIns(3)*P* (850150P; Avanti Polar Lipids, Inc.) and suspended at 1 mg/ml by vortexing in 20 mM Hepes, pH 7.4, 150 mM NaCl, and 1 mM DTT, then extruded through 200-nm pore-size filters using a mini-extruder (Avanti Polar Lipids, Inc.).

His-tag fusion vector of Mvp1 was made by amplifying the MVP1 ORF as a BglII–XhoI fragment of from wild-type genomic DNA as a template. The amplified product was cloned in-frame into BamHI and XhoI sites of vector pET28a (EMD Millipore), and the resulting plasmid was sequenced. The plasmid was transformed into *Escherichia coli* BL21 and expressed by auto-induction as described previously (Studier, 2005). In brief, plasmids were transformed into BL21(DE3)-competent cells and grown in Terrific Broth containing the appropriate antibiotics in baffled flasks filled to 20% of the total volume. Sterile lactose solution was added to a final concentration of 0.2% and cultures were grown at 37°C for 4 h, then shifted to room temperature for 20 h. Recombinant Mvp1 contained a C-terminal His-tag and was purified using an ÄKTAprime Plus fast protein liquid chromatography (FPLC) system (GE Healthcare) equipped with a 1-ml His-Trap HP column, followed by buffer exchange into tubulation/vesiculation assay buffer. Purified protein concentration was quantified by BCA assay (Thermo Fisher Scientific).

For tubule/vesiculation assays, 5 µg liposomes were incubated with 0, 10, or 20 µM recombinant Mvp1 (10 µl final volume) for 30 min at 30°C and spotted onto a carbon-coated copper mesh grid. Liposomes were negative stained by 1% uranyl acetate and analyzed on a transmission

Downloaded from jcb.rupress.org on June 24, 2015

Published February 24, 2014

electron microscope (Tecnai F12; FEI Company). Tubules and vesicle diameters were quantified in ImageJ analysis software as an average of three measurements along the tubule or two measurements tangentially across the coated vesicle.

Online supplemental material

Fig. S1 shows Mvp1 endosome localization is dependent upon PtdIns3*P* binding and that Mvp1 partially colocalizes with sorting nexins, Vps17, Snx3, and Snx4. Fig. S2 shows Vps1-GFP is not fully functional but colocalizes with late endosome marker Cherry-Ypt7 or Did2-mKate in diploid strains carrying one untagged and one GFP-tagged *VPS1* allele. Additionally, Vps1-GFP Did2-mkate co-decorated endosomes were dramatically reduced in cells lacking Mvp1. Video 1 is a time-lapse video of Mvp1-GFP demonstrating the dynamic nature of the tubular endosomal network. Video 2 shows a tomographic series and model of *vps1Δ* cells. Online supplemental material is available at http://www.jcb.org/cgi/content/full/jcb.201309084/DC1.

We are grateful to. S. Sever for Vps1 reagents; to G. Payne for providing 2xGFP and 2xmRFP cassettes; to C. Danson and P. Cullen (University of Bristol) for sharing unpublished information regarding SNX8; to our colleagues for discussions and critical reading of the manuscript; and to M. Burd for secretarial help. We would like to acknowledge the Boulder Laboratory for 3D Electron Microscopy of Cells and Yale School of Medicine Center for Cellular and Molecular Imaging for the EM scopes we used for this study.

This work was supported by grants from the National Institutes of Health to G. Odorizzi (GM065505) and to C.G. Burd (GM060221).

The authors declare no competing financial interests.

Submitted: 17 September 2013
Accepted: 24 January 2014

References

Allison, R., J.H. Lumb, C. Fassier, J.W. Connell, D. Ten Martin, M.N. Seaman, J. Hazan, and E. Reid. 2013. An ESCRT-spastin interaction promotes fission of recycling tubules from the endosome. *J. Cell Biol.* 202:527–543. http://dx.doi.org/10.1083/jcb.201211045

Alpadi, K., A. Kulkarni, S. Namjoshi, S. Srinivasan, K.H. Sippel, K. Ayscough, M. Zieger, A. Schmidt, A. Mayer, M. Evangelista, et al. 2013. Dynamin-SNARE interactions control trans-SNARE formation in intracellular membrane fusion. *Nat Commun*. 4:1704. http://dx.doi.org/10.1038/ncomms2724

Bonangelino, C.J., E.M. Chavez, and J.S. Bonifacino. 2002. Genomic screen for vacuolar protein sorting genes in *Saccharomyces cerevisiae*. *Mol. Biol. Cell*. 13:2486–2501. http://dx.doi.org/10.1091/mbc.02-01-0005

Bonifacino, J.S., and R. Rojas. 2006. Retrograde transport from endosomes to the trans-Golgi network. *Nat. Rev. Mol. Cell Biol.* 7:568–579. http://dx.doi.org/10.1038/nrm1985

Boucrot, E., A. Pick, G. Çamdere, N. Liska, E. Evergren, H.T. McMahon, and M.M. Kozlov. 2012. Membrane fission is promoted by insertion of amphipathic helices and is restricted by crescent BAR domains. *Cell*. 149:124–136. http://dx.doi.org/10.1016/j.cell.2012.01.047

Burston, H.E., L. Maldonado-Báez, M. Davey, B. Montpetit, C. Schluter, B. Wendland, and E. Conibear. 2009. Regulators of yeast endocytosis identified by systematic quantitative analysis. *J. Cell Biol.* 185:1097–1110. http://dx.doi.org/10.1083/jcb.200811116

Carlton, J., M. Bujny, B.J. Peter, V.M. Oorschot, A. Rutherford, H. Mellor, J. Klumperman, H.T. McMahon, and P.J. Cullen. 2004. Sorting nexin-1 mediates tubular endosome-to-TGN transport through coincidence sensing of high- curvature membranes and 3-phosphoinositides. *Curr. Biol.* 14:1791–1800. http://dx.doi.org/10.1016/j.cub.2004.09.077

Costanzo, M., A. Baryshnikova, J. Bellay, Y. Kim, E.D. Spear, C.S. Sevier, H. Ding, J.L. Koh, K. Toufighi, S. Mostafavi, et al. 2010. The genetic landscape of a cell. *Science*. 327:425–431. http://dx.doi.org/10.1126/science.1180823

Deloche, O., and R.W. Schekman. 2002. Vps10p cycles between the TGN and the late endosome via the plasma membrane in clathrin mutants. *Mol. Biol. Cell*. 13:4296–4307. http://dx.doi.org/10.1091/mbc.02-07-0105

Derivery, E., C. Sousa, J.J. Gautier, B. Lombard, D. Loew, and A. Gautreau. 2009. The Arp2/3 activator WASH controls the fission of endosomes through a large multiprotein complex. *Dev. Cell*. 17:712–723. http://dx.doi.org/10.1016/j.devcel.2009.09.010

Dyve, A.B., J. Bergan, A. Utskarpen, and K. Sandvig. 2009. Sorting nexin 8 regulates endosome-to-Golgi transport. *Biochem. Biophys. Res. Commun.* 390:109–114. http://dx.doi.org/10.1016/j.bbrc.2009.09.076

Ekena, K., and T.H. Stevens. 1995. The *Saccharomyces cerevisiae* MVP1 gene interacts with VPS1 and is required for vacuolar protein sorting. *Mol. Cell. Biol.* 15:1671–1678.

Frost, A., M.G. Elgort, O. Brandman, C. Ives, S.R. Collins, L. Miller-Vedam, J. Weibezahn, M.Y. Hein, I. Poser, M. Mann, et al. 2012. Functional repurposing revealed by comparing *S. pombe* and *S. cerevisiae* genetic interactions. *Cell*. 149:1339–1352. http://dx.doi.org/10.1016/j.cell.2012.04.028

Gallop, J.L., C.C. Jao, H.M. Kent, P.J. Butler, P.R. Evans, R. Langen, and H.T. McMahon. 2006. Mechanism of endophilin N-BAR domain-mediated membrane curvature. *EMBO J.* 25:2898–2910. http://dx.doi.org/10.1038/sj.emboj.7601174

Geuze, H.J., J.W. Slot, G.J. Strous, H.F. Lodish, and A.L. Schwartz. 1983. Intracellular site of asialoglycoprotein receptor-ligand uncoupling: double-label immunoelectron microscopy during receptor-mediated endocytosis. *Cell*. 32:277–287. http://dx.doi.org/10.1016/0092-8674(83)90518-4

Giddings, T.H. 2003. Freeze-substitution protocols for improved visualization of membranes in high-pressure frozen samples. *J. Microsc.* 212:53–61. http://dx.doi.org/10.1046/j.1365-2818.2003.01228.x

Gomez, T.S., and D.D. Billadeau. 2009. A FAM21-containing WASH complex regulates retromer-dependent sorting. *Dev. Cell*. 17:699–711. http://dx.doi.org/10.1016/j.devcel.2009.09.009

Hayden, J., M. Williams, A. Granich, H. Ahn, B. Tenay, J. Lukehart, C. Highfill, S. Dobard, and K. Kim. 2013. Vps1 in the late endosome-to-vacuole traffic. *J. Biosci.* 38:73–83. http://dx.doi.org/10.1007/s12038-012-9295-2

Hettema, E.H., M.J. Lewis, M.W. Black, and H.R. Pelham. 2003. Retromer and the sorting nexins Snx4/41/42 mediate distinct retrieval pathways from yeast endosomes. *EMBO J.* 22:548–557. http://dx.doi.org/10.1093/emboj/cdg062

Hopkins, C.R. 1983. Intracellular routing of transferrin and transferrin receptors in epidermoid carcinoma A431 cells. *Cell*. 35:321–330. http://dx.doi.org/10.1016/0092-8674(83)90235-0

Horazdovsky, B.F., G.R. Busch, and S.D. Emr. 1994. VPS21 encodes a rab5-like GTP binding protein that is required for the sorting of yeast vacuolar proteins. *EMBO J.* 13:1297–1309.

Koh, J.L., H. Ding, M. Costanzo, A. Baryshnikova, K. Toufighi, G.D. Bader, C.L. Myers, B.J. Andrews, and C. Boone. 2010. DRYGIN: a database of quantitative genetic interaction networks in yeast. *Nucleic Acids Res.* **38**(Database, Database issue):D502–D507. http://dx.doi.org/10.1093/nar/gkp820

Kremer, J.R., D.N. Mastronarde, and J.R. McIntosh. 1996. Computer visualization of three-dimensional image data using IMOD. *J. Struct. Biol.* 116:71–76. http://dx.doi.org/10.1006/jsbi.1996.0013

Liu, T.T., T.S. Gomez, B.K. Sackey, D.D. Billadeau, and C.G. Burd. 2012. Rab GTPase regulation of retromer-mediated cargo export during endosome maturation. *Mol. Biol. Cell*. 23:2505–2515. http://dx.doi.org/10.1091/mbc.E11-11-0915

Llorente, A., A. Rapak, S.L. Schmid, B. van Deurs, and K. Sandvig. 1998. Expression of mutant dynamin inhibits toxicity and transport of endocytosed ricin to the Golgi apparatus. *J. Cell Biol.* 140:553–563. http://dx.doi.org/10.1083/jcb.140.3.553

Longtine, M.S., A. McKenzie III, D.J. Demarini, N.G. Shah, A. Wach, A. Brachat, P. Philippsen, and J.R. Pringle. 1998. Additional modules for versatile and economical PCR-based gene deletion and modification in *Saccharomyces cerevisiae*. *Yeast*. 14:953–961. http://dx.doi.org/10.1002/(SICI)1097-0061(199807)14:10<953::AID-YEA293>3.0.CO;2-U

Luo, W., and A. Chang. 2000. An endosome-to-plasma membrane pathway involved in trafficking of a mutant plasma membrane ATPase in yeast. *Mol. Biol. Cell*. 11:579–592. http://dx.doi.org/10.1091/mbc.11.2.579

Mari, M., M.V. Bujny, D. Zeuschner, W.J. Geerts, J. Griffith, C.M. Petersen, P.J. Cullen, J. Klumperman, and H.J. Geuze. 2008. SNX1 defines an early endosomal recycling exit for sortilin and mannose 6-phosphate receptors. *Traffic*. 9:380–393. http://dx.doi.org/10.1111/j.1600-0854.2007.00686.x

Mastronarde, D.N. 2005. Automated electron microscope tomography using robust prediction of specimen movements. *J. Struct. Biol.* 152:36–51. http://dx.doi.org/10.1016/j.jsb.2005.07.007

Nickerson, D.P., M. West, R. Henry, and G. Odorizzi. 2010. Regulators of Vps4 ATPase activity at endosomes differentially influence the size and rate of formation of intralumenal vesicles. *Mol. Biol. Cell*. 21:1023–1032. http://dx.doi.org/10.1091/mbc.E09-09-0776

Nicoziani, P., F. Vilhardt, A. Llorente, L. Hilout, P.J. Courtoy, K. Sandvig, and B. van Deurs. 2000. Role for dynamin in late endosome dynamics and trafficking of the cation-independent mannose 6-phosphate receptor. *Mol. Biol. Cell*. 11:481–495. http://dx.doi.org/10.1091/mbc.11.2.481

Peter, B.J., H.M. Kent, I.G. Mills, Y. Vallis, P.J. Butler, P.R. Evans, and H.T. McMahon. 2004. BAR domains as sensors of membrane curvature: the amphiphysin BAR structure. *Science*. 303:495–499. http://dx.doi.org/10.1126/science.1092586

Peters, C., T.L. Baars, S. Bühler, and A. Mayer. 2004. Mutual control of membrane fission and fusion proteins. *Cell*. 119:667–678. http://dx.doi.org/10.1016/j.cell.2004.11.023

Puthenveedu, M.A., B. Lauffer, P. Temkin, R. Vistein, P. Carlton, K. Thorn, J. Taunton, O.D. Weiner, R.G. Parton, and M. von Zastrow. 2010.

Downloaded from jcb.rupress.org on June 24, 2015

Published February 24, 2014

Sequence-dependent sorting of recycling proteins by actin-stabilized endosomal microdomains. *Cell*. 143:761–773. http://dx.doi.org/10.1016/j.cell.2010.10.003

Raymond, C.K., I. Howald-Stevenson, C.A. Vater, and T.H. Stevens. 1992. Morphological classification of the yeast vacuolar protein sorting mutants: evidence for a prevacuolar compartment in class E *vps* mutants. *Mol. Biol. Cell*. 3:1389–1402. http://dx.doi.org/10.1091/mbc.3.12.1389

Roth, T.F., and K.R. Porter. 1964. Yolk protein uptake in the oocyte of the mosquito *Aedes aegypti.* L. *J. Cell Biol.* 20:313–332. http://dx.doi.org/10.1083/jcb.20.2.313

Roux, A., G. Koster, M. Lenz, B. Sorre, J.B. Manneville, P. Nassoy, and P. Bassereau. 2010. Membrane curvature controls dynamin polymerization. *Proc. Natl. Acad. Sci. USA*. 107:4141–4146. http://dx.doi.org/10.1073/pnas.0913734107

Schmid, E.M., and H.T. McMahon. 2007. Integrating molecular and network biology to decode endocytosis. *Nature*. 448:883–888. http://dx.doi.org/10.1038/nature06031

Seaman, M.N., E.G. Marcusson, J.L. Cereghino, and S.D. Emr. 1997. Endosome to Golgi retrieval of the vacuolar protein sorting receptor, Vps10p, requires the function of the VPS29, VPS30, and VPS35 gene products. *J. Cell Biol.* 137:79–92. http://dx.doi.org/10.1083/jcb.137.1.79

Seaman, M.N., J.M. McCaffery, and S.D. Emr. 1998. A membrane coat complex essential for endosome-to-Golgi retrograde transport in yeast. *J. Cell Biol.* 142:665–681. http://dx.doi.org/10.1083/jcb.142.3.665

Sherman, F., G.R. Fink, and L.W. Lawrence. 1979. Methods in yeast genetics: A laboratory manual. Cold Spring Harbor Laboratory Press, Cold Spring Harbor, NY. 73 pp.

Smaczynska-de Rooij, I.I., E.G. Allwood, S. Aghamohammadzadeh, E.H. Hettema, M.W. Goldberg, and K.R. Ayscough. 2010. A role for the dynamin-like protein Vps1 during endocytosis in yeast. *J. Cell Sci.* 123:3496–3506. http://dx.doi.org/10.1242/jcs.070508

Smaczynska-de Rooij, I.I., E.G. Allwood, R. Mishra, W.I. Booth, S. Aghamohammadzadeh, M.W. Goldberg, and K.R. Ayscough. 2012. Yeast dynamin Vps1 and amphiphysin Rvs167 function together during endocytosis. *Traffic*. 13:317–328. http://dx.doi.org/10.1111/j.1600-0854.2011.01311.x

Studier, F.W. 2005. Protein production by auto-induction in high density shaking cultures. *Protein Expr. Purif.* 41:207–234. http://dx.doi.org/10.1016/j.pep.2005.01.016

Teasdale, R.D., and B.M. Collins. 2012. Insights into the PX (phox-homology) domain and SNX (sorting nexin) protein families: structures, functions and roles in disease. *Biochem. J.* 441:39–59. http://dx.doi.org/10.1042/BJ20111226

Traer, C.J., A.C. Rutherford, K.J. Palmer, T. Wassmer, J. Oakley, N. Attar, J.G. Carlton, J. Kremerskothen, D.J. Stephens, and P.J. Cullen. 2007. SNX4 coordinates endosomal sorting of TfnR with dynein-mediated transport into the endocytic recycling compartment. *Nat. Cell Biol.* 9:1370–1380. http://dx.doi.org/10.1038/ncb1656

van Weering, J.R., R.B. Sessions, C.J. Traer, D.P. Kloer, V.K. Bhatia, D. Stamou, S.R. Carlsson, J.H. Hurley, and P.J. Cullen. 2012a. Molecular basis for SNX-BAR-mediated assembly of distinct endosomal sorting tubules. *EMBO J.* 31:4466–4480. http://dx.doi.org/10.1038/emboj.2012.283

van Weering, J.R., P. Verkade, and P.J. Cullen. 2012b. SNX-BAR-mediated endosome tubulation is co-ordinated with endosome maturation. *Traffic*. 13:94–107. http://dx.doi.org/10.1111/j.1600-0854.2011.01297.x

Wemmer, M., I. Azmi, M. West, B. Davies, D. Katzmann, and G. Odorizzi. 2011. Bro1 binding to Snf7 regulates ESCRT-III membrane scission activity in yeast. *J. Cell Biol.* 192:295–306. http://dx.doi.org/10.1083/jcb.201007018

Wilsbach, K., and G.S. Payne. 1993. Vps1p, a member of the dynamin GTPase family, is necessary for Golgi membrane protein retention in *Saccharomyces cerevisiae*. *EMBO J.* 12:3049–3059.

Downloaded from jcb.rupress.org on June 24, 2015